Appl Petrochem Res (2017) 7:33–40
DOI 10.1007/s13203-017-0176-3

ORIGINAL ARTICLE

Effect of different precursor species on the metal dispersion of a Ni/γ-Al_2O_3 adsorbent for sulfur adsorption

Chi Zhang[1] · Yong-Ming Chai[1] · Chen-Guang Liu[1]

Received: 14 July 2016 / Accepted: 3 March 2017 / Published online: 25 March 2017

Abstract Nickel adsorbents supported on the γ-Al_2O_3 with different nickel precursor species were prepared by the incipient impregnation method to investigate the influence of different precursor species on the metal dispersion and the sulfur capacity of the adsorbents. The adsorbents were characterized by N_2 adsorption–desorption, H_2 temperature-programmed reduction (TPR), transmission electron microscopy (TEM), O_2–H_2 chemisorption, and FT-IR of adsorbed pyridine. The sulfur adsorption performance was investigated at ambient temperature and pressure. The results showed that adsorbent's metal dispersion and sulfur capacity were influenced significantly by the metal precursor species. The adsorbents prepared by nickel nitrate exhibited higher sulfur capacity and metal dispersion compared to the adsorbents prepared by nickel formate and nickel acetate. The higher performance of adsorbent prepared by nickel nitrate can be mainly attributed to the relatively more uniform metal dispersion and the smaller particle size of the nickel particles. This study demonstrates that the precursor species is an important factor for affecting the adsorption performance and provides a novel design idea of high metal dispersed catalysts.

Keywords Precursor species · Dry impregnation · Metal dispersion · Ni/γ-Al_2O_3 adsorbents

Introduction

As a result of environmental legislations set by the governments all over the world, the sulfur concentration of gasoline has been decreasing constantly these years [1]. However, for ultra-deep desulfurization (sulfur <10 μg/g) of gasoline, traditional hydrodesulfurization (HDS) is unsuitable [2]. For one thing, the hydrotreating unit requires more severe operation conditions to meet the standard of ultra-deep desulfurization. For another, the HDS process for ultra-deep desulfurization will result in an unacceptable loss of octane number [3]. Recently, selective adsorption desulfurization (SADS) has attracted increasing attention because of its visible advantages. Operation conditions of the SADS unit are mild, so equipment and operational capital expenditures are low. Moreover, there is nearly no octane number loss for gasoline desulfurization using the SADS process [4]. Hence, selective adsorption has been reported as an efficient way for desulfurization of gasoline. Nevertheless, due to vulnerability of SADS process, that is low sulfur capacity and short stability of the adsorbents, the process has not been industrialized up to now [5].

As a result of the advantages of SADS, efforts have been made to improve the metal dispersion and the stability of the adsorbent because of the positive correlation between metal dispersion and sulfur capacity based on the same metal loadings. Qiu [6] found that adding ethylene glycol into the precursor aqueous solution can promote the interaction of active metal with the support, which caused the formation of small metallic particles and high metal dispersion. Chang Hyun Ko [1] synthesized the nickel nanoparticles in solution in the presence of a capping agent, then the nickel particles

Electronic supplementary material The online version of this article (doi:10.1007/s13203-017-0176-3) contains supplementary material, which is available to authorized users.

✉ Chen-Guang Liu
cgliu@upc.edu.cn

[1] State Key Laboratory of Heavy Oil Processing, Key Laboratory of Catalysis, China National Petroleum Corporation (CNPC), China University of Petroleum, 66 West Changjiang Road, Qingdao 266580, Shandong, People's Republic of China

were incorporated into the support by sonication. Results showed that the method can maintain the particle sizes after calcination, but it is difficult to remove the capping agent completely from the adsorbent. Also, changing the calcination temperature of the catalyst, adding some titanium into the catalyst, and using the ethanol as the solvent rather than water, etc., were tried already [7, 8]. However, high temperature can dramatically destroy the pore structure of the support and result in the formation of the nickel alumina spinel. Other methods need expensive capping agents or complex preparation processes that are too difficult to apply in industry.

Ni/γ-Al_2O_3 catalyst is widely used in the petrochemical industry. The most common utilization of Ni/γ-Al_2O_3 catalyst is the methanation of CO and CO_2, where CO and CO_2 are reacted to methane by hydrogenation to product the synthesis nature gas [9, 10]. Furthermore, the Ni/γ-Al_2O_3 is used on the ultra-deep desulfurization for the feed of fuel-cell [11]. Also, Ni-based catalyst plays an important role in the field of hydrogenation for gasoline, diesel, and even heavy oil [12, 13].

Herein, we investigated the influences of different precursor species on metal dispersion and sulfur capacity of adsorbents. Three kinds of adsorbents synthesized by different nickel precursor species (nickel formate, nickel acetate, and nickel nitrate) and supported on the γ-Al_2O_3 were synthesized via the incipient impregnation method. The as-prepared adsorbents were characterized by nitrogen adsorption–desorption, temperature-programmed reduction (H_2-TPR), O_2–H_2 chemisorption, transmission electron microscopy (TEM), and FT-IR of adsorbed pyridine. Results show that adsorbent prepared by the nickel nitrate exhibits better performance compared to the adsorbents prepared by the nickel formate and nickel acetate precursors as a result of the smaller particle size and higher metal dispersion.

Experiment

Materials

γ-Al_2O_3 (surface area, 300 m^2/g; pore volume, 0.7 cm^3/g) was chosen as the support. Nickel formate, nickel acetate and nickel nitrate (analytical reagents) were purchased from Sinopharm Chemical Reagent Co. Ltd. Ammonium hydroxide was purchased form Xilong chemical Co. Ltd. All chemicals were used as received.

Adsorbents preparation

γ-Al_2O_3 (90 g, divided into three equal parts) was dried in the oven at 120 °C for 4 h. Simultaneously, Nickel formate (6.636 g), nickel acetate (11.104 g), and nickel nitrate (12.976 g) were dissolved in the deionized water and stirred for half an hour. Then, two cups of 13.8 mL ammonium hydroxide were added into nickel formate and nickel acetate solutions because the solubility of these two precursors was low and precipitates emerged. The Ni/γ-Al_2O_3 adsorbents were prepared by the incipient-wetness impregnation method. Thereafter, the adsorbents were obtained by drying in air for 12 h, drying in the oven at 120 °C for 4 h, and calcining in the muffle furnace at 300 °C for 4 h. In the end, the samples prepared by nickel formate, nickel acetate, and nickel nitrate were labeled as adsorbent-F, adsorbent-A, and adsorbent-N, respectively.

Adsorbent characterization

TPR was performed on a chemisorption analyzer (AutoChem 2905 HP). 0.1 g of each sample (dried and unreacted) was loaded in a U-shaped quartz glass tube. 50 mL/min of argon gas was passed through the tube for 20 min to remove the H_2O vapor in the pores of γ-Al_2O_3 at 60 °C first. Then, the oxide was reduced in a H_2/Ar (10% H_2) gas with a flow rate of 50 mL/min. The sample was heated to the experiment-defined temperature with a rate of 10 °C/min. A liquid nitrogen/isopropanol cold trap was necessary to condense the resulting water in the effluent.

O_2-H_2 chemisorption was performed at the temperature depending on the TPR measurement. A mixture of H_2 and Ar (10% H_2) gas was introduced into the quartz tube reactor by means of impulse at a frequency of 2 min^{-1}. The chromatographic peaks were recorded, and the experiment continued until the peak area remained unchanged. The liquid nitrogen/isopropanol cold trap was still necessary.

XRD measurements of the dried, solid, and powder samples were performed on an X'pert pro Philips diffractometer with Cu Kα radiation ($\lambda = 0.15406$ nm). The scanning range of 2θ was from 5 to 75° at scanning velocity of 10°/min. The step size was 0.0167° at 25 °C.

A micromeritics TriStar II (3020) N_2 adsorption and desorption analyzer was used to measure specific surface area (SSA) and pore structure properties. Specifically, the SSA was measured via BET isotherm and the pore structure properties was measured following the BJH method from the desorption isotherms. Samples were degassed at 250 °C and 0.1 mbar for 6 h before nitrogen adsorption.

TEM characterization was performed on the reduced adsorbents. The samples were grinded to a powder and then dispersed uniformly in ethanol. A drop of the suspension was then placed onto a carbon–coated copper grid in the electron microscope (F-20 FasTEMm FEI) operated at 200 kV.

The Bruker VERTEX 70 spectrometer was used to identify the acid types and quantities of the as-prepared

adsorbents. Before measurement, samples were dried in 200 °C for 1 h to remove the vapor in the pores. The scan range of equipment was 400–4000 cm, and the resolution ratio was 2 cm^{-1}.

Adsorbents performance evaluation

The performance of the adsorbents was evaluated in a 10 mL fixed-bed micro-reactor.

The feedstock was a mixture of n-hexane (10 wt%), cyclohexane (80 wt%), and n-heptane (10 wt%). The mass fraction of thiophene in feedstock was 0.0102 wt% and the density of the mixture was 0.7738 g/cm^3. The adsorbents with the size of 20–40 mesh were loaded in the reactor and pre-reduced in H_2 at 450 °C for 4 h before the adsorption. After cooling to room temperature in hydrogen, the liquid feed was introduced into the reactor at a certain flow rate of 12 mL/h at ambient temperature. To make the liquid contact the adsorbents fully, the flow direction was from the bottom to the top of the reactor and the liquid product was collected on the top. The concentration of thiophene in the outlet liquid was measured by a GC chromatograph equipped with a FPD detector and a HP-5 column. The temperature-rising speed was 1 °C/min and the flow velocity of gas was 0.1 mL/min. The adsorbent was considered to be deactivated once the sulfur capacity in the outlet product was consistent with that in the feed. The calculation formulas of the breakthrough sulfur capacity and the metal dispersion of the adsorbent are described below:

$$\text{Breakthrough sulfur capacity: } V(S) = \frac{S(\text{wt\%}) \times \rho \times V}{m} \times 100\% \quad (1)$$

$$\text{Metal dispersion: } D = \frac{V(S) \times Ma}{F \times Ms} \times 100\% \quad (2)$$

Equations (1) and (2) assume that the sulfur atom in the thiophene molecule interacts with metallic nickel directly by the lone pair electrons. Where $V(S)$ stands for the breakthrough sulfur capacity and D stands for the metal dispersion. S (wt%) signifies the sulfur capacity of the feed, μg/g. ρ (g/cm^3) stands for the density of the feed and V (mL) stands for the volume of the product after the adsorption. F means the loading of the NiO and m (g) stands for the weight of the adsorbent which loaded in the reactor. Ms and Ma (g/mol) stands for the molar mass of the sulfur and the NiO.

Results and discussion

H_2-TPR

Figure 1 shows the H_2-TPR patterns of the as-prepared Ni adsorbents supported on the γ-Al_2O_3 with different precursor species. The reduction profiles of the adsorbents can

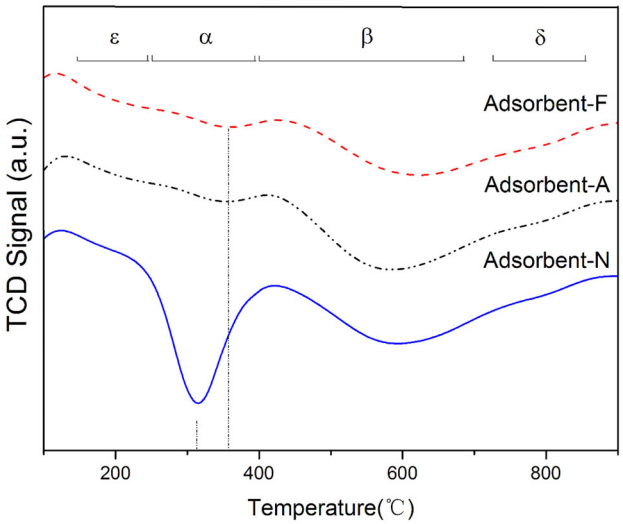

Fig. 1 TPR profiles of adsorbents with different precursor species-adsorbent-F, adsorbent-A, adsorbent-N

be classified into four bands, band ε, band α, band β, and band δ. The peaks in band ε at around 200 °C are attributed to the highly dispersed nickel species, such as Ni_2O_3 and NiO on the surface of the adsorbents. In the band α, the peaks between 250 and 440 °C are attributed to the reduction of the bulk Ni_2O_3 and NiO [14]. In the band β, the broad peaks between 440 and 700 °C are attributed to the reduction of the strong interaction between the nickel oxide and the support. The peaks in the band δ from 750 to 850 °C belong to the reduction of the spinel phase of the nickel aluminate.

Figure 1 shows that profiles of adsorbent-F and adsorbent-A are similar whereas adsorbent-N profile is different. In the three samples, the main nickel species are the bulk Ni_2O_3 or NiO and the nickel oxide interacted strongly with the support (band α and band β) [14]. Simultaneously, on the surface of the adsorbent, there are a little highly dispersed nickel oxides and nickel aluminates that are difficult to reduce. Since the reduction temperature in the fixed bed reactor was 450 °C, only nickel species in band ε and band α can be reduced to the metal phase. In the band α, the temperature of adsorbent-F and adsorbent-A peaks are both 360 °C while the reduction peak temperature of Adsorbent-N is 315 °C. The lower reduction temperature of Adsorbent-N signifies that the bulk nickel oxide on the Adsorbent-N is easier to reduce compared to those on the other two adsorbents. Hence, the active nickel oxide particle size (average size) of the Adsorbent-N is the smallest one among the three adsorbents, indicating that the metal dispersion of the Adsorbent-N is the best [1]. The result matches with the adsorbent evaluation experiment result well. On the other hand, in the band α, the peak area of Adsorbent-F is like to that of adsorbent-A. The peak area of Adsorbent-N is the largest of the three samples and much

bigger than those of the former two samples, indicating that Adsorbent-N consumes more H_2 during the TPR reaction. The main reason is that the nickel particles on the surface of Adsorbent-N are smaller and disperse more uniformly than those on the surface of adsorbent-F and adsorbent-A. Thus, there are more nickel atoms exposed on the surface of Adsorbent-N and result in consuming more H_2. Another reason is that CO is generated while the nickel format and the nickel acetate decompose in high temperature. And CO can partly reduce the nickel oxide to the metal phase in high temperature so that adsorbent-F and adsorbent-A consume less hydrogen than Adsorbent-N.

O_2-H_2 chemisorption

The metal dispersion was measured by O_2–H_2 chemisorption method. A hydrogen diluted stream (H_2 10%, Ar 90%) was introduced into the quartz tube reactor by means of pulse. The chromatographic peaks were recorded by computer, and the experiment was not finished until the peak area kept unchanged. In this way, the nickel atom numbers on the surface of the adsorbent were obtained via calculating the volume of hydrogen consumed. The process of O_2–H_2 chemisorption was that the metallic nickel was oxidized to NiO by O_2 and then reduced to metallic nickel by H_2. Eventually, the nickel adsorbed the hydrogen atoms and the band exited in the form of adsorption affinity. The formulas are as follow:

$$O_2 + 2Ni \rightarrow 2NiO \quad (3)$$

$$2NiO + 3H_2 \rightarrow 2Ni\text{-}H + 2H_2O \quad (4)$$

Formulas (3) and (4) showed that the mole ratio of H_2 which is assumed and nickel on the surface of the adsorbent is 3:2. Thereby, the calculation method of metal dispersion is deduced:

Metal dispersion (R):

$$R = \frac{N_{(Ni)}}{N_{(Ni)_{total}}} \quad (5)$$

$$N_{(Ni)} = \frac{2N_{(H_2)}}{3} = \frac{2(nV - V_1)P}{3RT} \quad (6)$$

Where $N_{(Ni)}$ signifies the mole number of nickel on the surface of the adsorbent and $N_{(Ni)\ total}$ means the total mole number of nickel-based adsorbent. $N_{(H2)}$ stands for the total mole number of hydrogen used during the process. V means the volume of hydrogen introduced into the reactor for each time ($V = 0.\ 058$ mL). V_1 signifies the volume of hydrogen unreacted with the nickel oxide (the total area of the characteristic peaks and the value is gained by integration) and P stands for the pressure of the system at that time, that is atmospheric pressure. T stands for the temperature of system during the reaction (383.15 K) and R is 8.314 J/(mol K). The meaning of n in Eq. (6) is the times of pulse, which value is the number of characteristic peaks (n can be obtained in O_2–H_2 chemisorption titration patterns in support material). The calculation results of metal dispersion are shown in Table 2.

Table 1 Metal dispersion of Ni-based adsorbents by O_2–H_2 Chemisorption method

Adsorbent	Adsorbent-F	Adsorbent-A	Adsorbent-N
Metal dispersion	5.47%	13.5%	15.1%
Stand deviation (10^{-4})	7.33	6.39	5.11

Table 1 shows that the metal dispersion of adsorbent-F, adsorbent-A, and adsorbent-N are 5.47, 13.5, and 15.1%, respectively. The result is in line with other characterization results and experiment evaluation result. However, the metal dispersion values of adsorbents by O_2–H_2 chemisorption are much higher than those by evaluation experiments. The differences are attributed to three main reasons. First, the size of a thiophene molecule is much larger than that of a hydrogen molecule so that there are some nickel particles in narrow places that thiophene molecules have difficulties contacting with while hydrogen molecules can do that easily. Second, thiophene molecules interact with nickel particles via several methods, such as end-on adsorption, lie-down adsorption, and bridge adsorption [15, 16]. That is, thiophene molecules interact with one, two, or even more metal particles but hydrogen contacts only one metal particle. In the end, the result of evaluation experiment assumes that the sulfur atom in the thiophene molecule interacts with metallic nickel directly by the lone pair electrons, but actually there are many contact methods between thiophene and metal nickel atoms. Therefore, the metal dispersion results obtained by O_2–H_2 chemisorption are much higher than those obtained by evaluation experiments.

FT–IR characterization of adsorbed pyridine

To identify the acid types and quantities of the adsorbents prepared by three different precursor species, the FT–IR spectra of pyridine adsorbed on the as-prepared adsorbents in the wave number ranging from 1800 to 1300 cm^{-1} were measured and the results are shown in Fig. 2. The peaks at 1540 and 1445 cm^{-1} correspond to those specific to the pyridine molecules chemisorbed on Bronsted and Lewis acid sites, respectively [17]. The band at 1485 cm^{-1} is ascribed to the adsorbate on both Bronsted and Lewis acid sites. Fan studied the acidity of Al_2O_3, the medium Lewis acid site occupied the most acid sites, but there were no Bronsted acid sites [18]. Each line in Fig. 2 shows that the most acid sites are the medium Lewis sites. The Bronsted acid sites are very

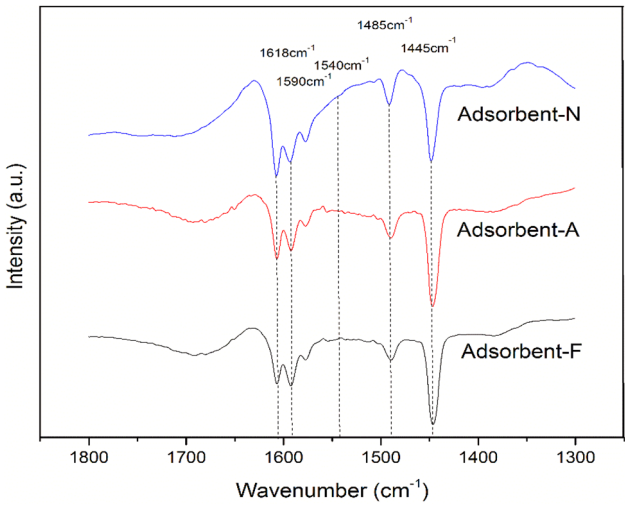

Fig. 2 Acid-type distribution of adsorbents obtained by the Py-IR spectra

little in all of the adsorbents from the Fig. 2, though the profile of adsorbent-N shows a small signal of Bronsed acid site. The intensity of Peaks at 1445, 1590 and 1618 cm^{-1} are similar. However, the intensity of peaks at 1485 cm^{-1} are discrepant. It is visible that characterization peak intensity of adsorbent-N is stronger than those of the other two adsorbents. Thiophene molecule is Lewis base due to the existence of lone pair electrons. Therefore, the relationship between the sulfur capacity of adsorbent and acid sites is positive correlation, that is the more acid sites, the more sulfur capacity. So, the result of Py-IR shows that adsorbent-N have more Lewis acid sites and hence the performance of the adsorbent-N is better. The result agrees with other characterization and experiment results.

TEM

Figure 3a–c show the TEM images of the adsorbents prepared by three different precursor species (the adsorbents were reduced at 450 °C for 4 h before the TEM characterization). The special structure of γ-Al_2O_3 is observed clearly from Fig. 3 and the black points in the images signify the metallic nickel particles. The images in Fig. 3 indicate that the metallic nickel particles disperse more uniformly in images of adsorbent-A and adsorbent-N while the distribution of metallic nickel particles of Adsorbent-F is more concentrated. Thereafter, the average metallic nickel particles radius are obtained by Gatan Digital Micrograph Suite (GMS) software. 200 nickel particles on each adsorbent are measured and the particle diameters distribution are shown in Fig. 4. Simultaneously, the average nickel diameters of adsorbents are calculated and shown in Fig. 3.

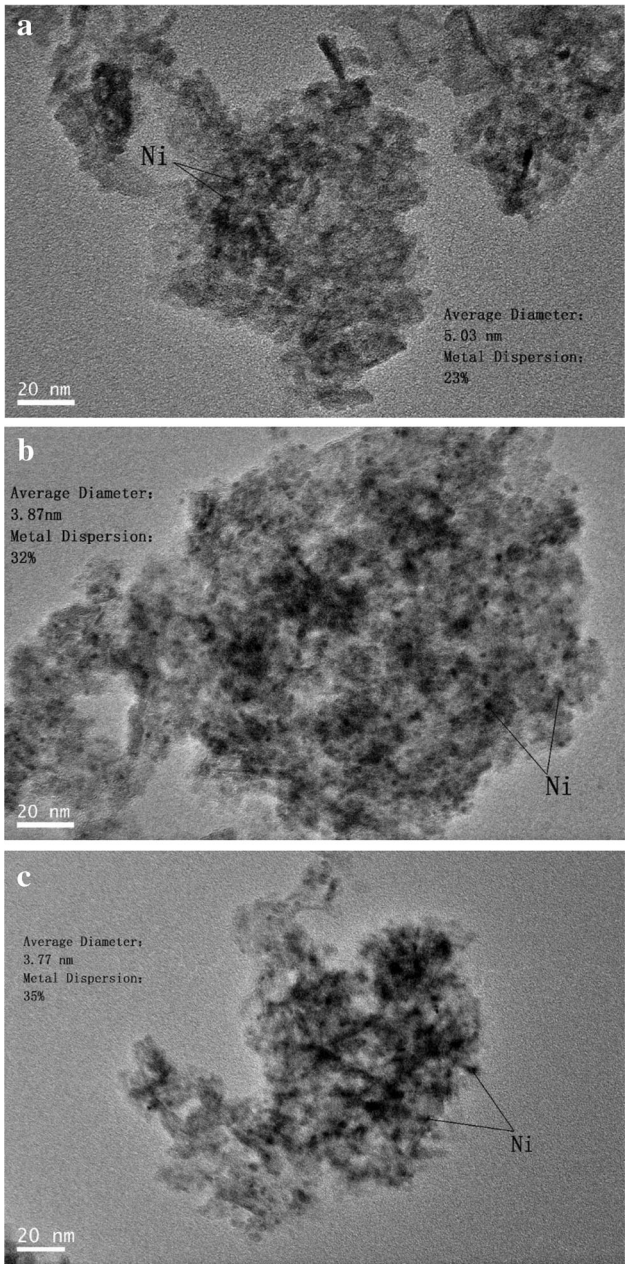

Fig. 3 TEM images of adsorbents with different precursors: **a** adsorbent-F, **b** adsorbent-A, **c** adsorbent-N

Figure 4 shows the metallic nickel particle radius distribution of as-prepared adsorbents. Particles of metallic nickel with the size of 1–8 nm are dispersed on the support. Result shows that the average particle radius of Adsorbent-F is the largest. The particle radius of adsorbent-A is close to that of adsorbent-N and the particle radius of adsorbent-N is the smallest. Namely that the metal dispersion of adsorbent-F is the worst. The adsorbent-N metal dispersion is the best and the metal dispersion of adsorbent-A is similar to that of adsorbent-N.

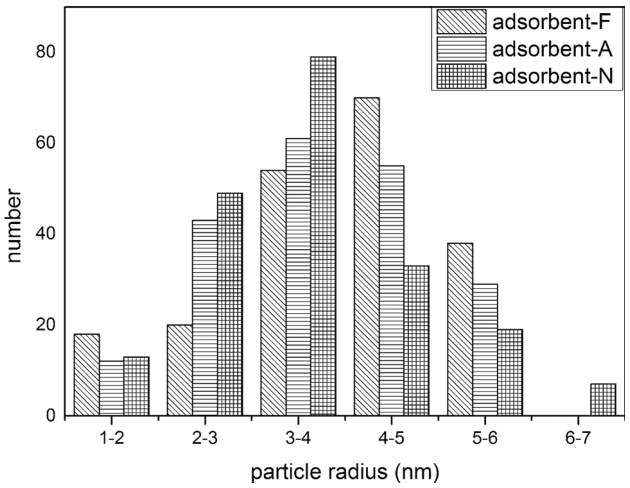

Fig. 4 The metallic nickel radius distribution of adsorbents prepared by three different precursor species

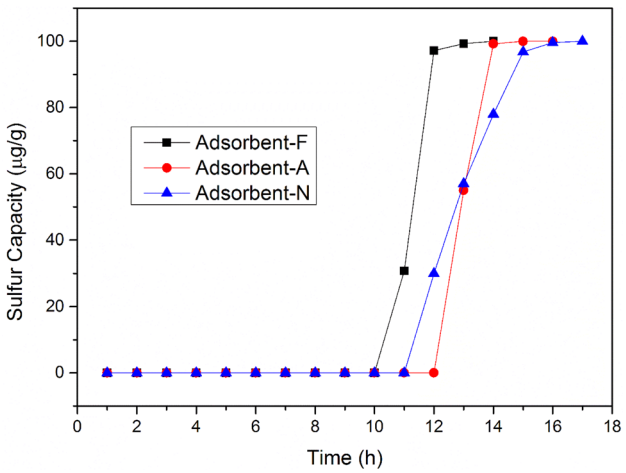

Fig. 5 Breakthrough sulfur capacity of different adsorbents

Scholten researched the relationship between the metal dispersion and average particle sizes of several kinds of metals and the result are utilized here [19]. Thereafter, the value of corresponding metal dispersion of the as-prepared adsorbents are obtained and the result is also shown in Fig. 3.

The nickel particles were composed of several nickel crystals. For Adsorbent-N, smaller nickel particles are observed in the spaces of the γ-Al_2O_3. The results confirmed that nickel nitrate precursors were distributed more uniformly at the beginning of the preparation and prevented the nickel species from growing into larger nickel particles during the calcination and high temperature reduction process, as compared to the other two nickel precursor species [20]. However, the metal dispersion results measured by TEM were different with the O_2–H_2 chemisorption results. The main reason was that the mechanism of the two measurements were fundamentally different. For TEM characterization, the bonds of points (nickel particles) were distinguished via eyes. Moreover, the curve of metal dispersion and average particle size was an experimental curve, so the errors were unavoidable. Thus, there were differences between results obtained by TEM and O_2–H_2 chemisorption method.

Adsorbent evaluation experiment

Figures 5 and 5 (supplementary material) shows the breakthrough sulfur capacity of adsorbents prepared by different precursor species. While the total volume of product in the outlet is 108 mL, the sulfur capacity in the liquid is still so little that the FPD detector cannot get the sulfur signal for all three samples. However, for Adsorbent-F, the sulfur signal is obtained by the detector while the product volume is 120 mL and the profile reaches a platform when the liquid volume is 132 mL. The platform means that the sulfur capacity of the product will not change with the liquid volume. That is, the adsorbent is deactivated. For adsorbent-A, the profile changes at $V = 144$ mL and reaches a platform when the liquid volume is 168 mL. The profile of Adsorbent-N is different, the sulfur signal appeared when $V = 132$ mL and reaches a platform when the product volume is 180 mL. The slope of the Adsorbent-N curve is smaller than those of the other two adsorbents. The main reasons are that the Adsorbent-N particle size is smaller and the metal nanoparticles disperse more uniformly compared to the adsorbent-F and the adsorbent-A.

Results of breakthrough sulfur capacity and metal dispersion of adsorbents calculated through Eqs. (1) and (2) are listed in Table 2.

The calculation results show that the breakthrough sulfur capacity and metal dispersion of adsorbent-N are 0.174 and 4.05%, respectively. Both better than those of adsorbent-F (0.132, 3.09%) and adsorbent-A (0.161, 3.77%). The result identifies with characterization results. The phenomenon is attributed to the following reasons. First, because the size of nickel ammine ion is larger than that of nickel ion, the stereo-hindrance effect is bigger when nickel ammine ion diffuses in channels of the support compared to the nickel ion. Hence, nickel ion disperses more uniformly. Second, because of the former reason, the average distances among nickel particles of adsorbent-F and adsorbent-A are closer than that of the adsorbent-N resulting in the nickel particles of adsorbent-F and adsorbent-A aggregate together and convert to the larger particles more easily in high temperature, that is more easy to be sintered. Therefore, the nickel utilization rates of adsorbent-F and adsorbent-A are lower. Moreover, the metal dispersion and sulfur capacity of adsorbent-A are

Table 2 Sulfur capacity and metal dispersion of adsorbents

Adsorbent	Sulfur capacity (%)	Metal dispersion (%)
Adsorbent-F	0.132	3.09
Adsorbent-A	0.161	3.77
Adsorbent-N	0.174	4.05

Table 3 Pore structure properties of the adsorbents

Samples	S_{BET} (m^2/g)	Pore volume (cm^3/g)	Average pore diameter (nm)
Adsorbent-F	292	0.579	6.54
Adsorbent-A	274	0.566	7.36
Adsorbent-N	270	0.541	7.41

better than those of Adsorbent-F. The main reason is that the solubility of nickel formate is lower and the solution is not transparent enough though ammonium hydroxide is added. Namely that there are tiny particles in solution that cannot be distinguished by eyes. Whereas, the nickel acetate solution is clear so the distribution of nickel acetate in the support pores is better. Also, the calcination temperature of three adsorbents is 300 °C but the decomposition temperature of nickel formate is lower. Therefore, for adsorbent-F, the NiO particles aggregate together after the decomposition of nickel formate. So the metal dispersion and sulfur capacity of Adsorbent-N is the best in three adsorbents and the metal dispersion and sulfur capacity of adsorbent-A is better than that of adsorbent-F.

N_2 adsorption–desorption

The N_2 adsorption–desorption isotherms (Fig. 2) and pore size distributions (Fig. 3) of the as-prepared adsorbents are performed in the supplementary material and the corresponding structural parameters (average values of three measurements) are presented in Table 3. Figure 3 in the supplementary material shows that the as-prepared adsorbents show a type-IV isotherm with an obvious hysteresis loop at relative pressures (P/P_0) ranging from 0.5 to 0.9, which is typical for mesoporous materials [21]. The pore size distribution curves are shown in Fig. 4 (in supplementary material), it can be seen that the pore diameter corresponding to the peaks of adsorbent-F, adsorbent-A, and adsorbent-N increase in turn. Particularly, Table 3 shows that the specific surface area (SSA) and pore volume of adsorbent-F are the largest among the three kinds of adsorbents while the average pore diameter is the smallest. On the contrary, the SSA and pore volume of the adsorbent-N is the smallest and the average pore diameter is the largest. Simultaneously, the corresponding property parameters of the adsorbent-A are in-between of the other two adsorbents. After the calcination, the SSA and Pore volume of the adsorbent-N is the smallest but the average pore diameter is the largest. The result confirms that there are more effective metallic nickel particles distributed on the surface of the adsorbent-N rather than sintering or reacted to the nickel aluminum spinel compared to the other two adsorbents. Additionally, the size of effective nickel particles on the surface of the adsorbent-N is more uniform and the layer of the metallic nickel is thinner. Moreover, given the size of the thiophene molecule, its diffusion is expected to be hindered in the small pores, for this, the adsorbent-N could offer a better sulfur uptake during adsorption. Therefore, the sulfur capacity and the metal dispersion of the adsorbent-N should be higher than those of the adsorbent-F and adsorbent-A combined with other characterization.

Conclusion

Nickel adsorbents supported on the γ-Al_2O_3 with different nickel precursor species (nickel formate, nickel acetate, and nickel nitrate) were prepared by the incipient impregnation method with nickel loadings at 10%. The characterization results were identified by the adsorption experiments. Results indicated that precursor species significantly influenced the metal dispersion as well as the interaction between the nickel particles and γ-Al_2O_3 support. Furthermore, the nickel nitrate adsorbent exhibited better sulfur capacity, metallic dispersion compared to the nickel formate and nickel acetate adsorbents. This work demonstrates that the precursor species is an important factor to influence the sulfur capacity and the stability of the adsorbents for gasoline.

References

1. Ko CH, Park JG, Park JC, Song H, Han S-S, Kim J-N (2007) Surface status and size influences of nickel nanoparticles on sulfur compound adsorption. Appl Surf Sci 253:5864–5867
2. Hernández S, Solarino L, Orsello G, Russo N, Fino D, Saracco G, Specchia V (2008) Desulfurization processes for fuel cells systems. Int J Hydrogen Energy 33:3209–3214

3. Song C (2003) An overview of new approaches to deep desulfurization for ultra-clean gasoline, diesel fuel and jet fuel. Catal Today 86:211–263
4. Velu S, Ma X, Song C (2003) Selective adsorption for removing sulfur from jet fuel over zeolite-based adsorbents. Ind Eng Chem Res 42:5293–5304
5. Hernández-Maldonado AJ, Yang FH, Qi G, Yang RT (2005) Desulfurization of transportation fuels by π-complexation sorbents: Cu(I)-, Ni(II)-, and Zn(II)-zeolites. Appl Catal B 56:111–126
6. Qiu S, Zhang X, Liu Q, Wang T, Zhang Q, Ma L (2013) A simple method to prepare highly active and dispersed Ni/MCM-41 catalysts by co-impregnation. Catal Commun 42:73–78
7. Li C, Liu J, Gao W, Zhao Y, Wei M (2013) Ce-promoted Rh/TiO_2 heterogeneous catalysts towards ethanol production from syngas. Catal Lett 143:1247–1254
8. Song H, Wang J, Wang Z, Song H, Li F, Jin Z (2014) Effect of titanium content on dibenzothiophene HDS performance over Ni2P/Ti-MCM-41 catalyst. J Catal 311:257–265
9. Kester KB, Zagli E, Falconer JL (1986) Methanation of carbon monoxide and carbon dioxide on Ni/Al_2O_3 catalysts: effects of nickel loading. Appl Catal 22(2):311–319
10. Quincoces CE, Dicundo S, Alvarez AM, González MG (2001) Effect of addition of CaO on Ni/Al_2O_3 catalysts over CO_2 reforming of methane. Mater Lett 50(1):21–27
11. Sun J, Qiu XP, Wu F, Zhu WT (2005) H2 from steam reforming of ethanol at low temperature over Ni/Y_2O_3, Ni/La_2O_3 and Ni/Al_2O_3 catalysts for fuel-cell application. Int J Hydrogen Energy 30(4):437–445
12. Castaño P, Pawelec B, Fierro JLG, Arandes JM, Bilbao J (2007) Enhancement of pyrolysis gasoline hydrogenation over Pd-promoted Ni/SiO_2–Al_2O_3, catalysts. Fuel 86(15):2262–2274
13. Iwamoto R, Nozaki T, Uchikawa K (2002) Hydrogenation catalyst and method of hydrogenating heavy oil US, US 6398950 B1
14. Hu CW, Jie Y, Yang HQ, Yu C, Tian AM (1997) On the inhomogeneity of low nickel loading methanation. Catal J Catal 166:1–7
15. Raybaud P, Hafner J, Kresse G, Toulhoat H (1998) Adsorption of Thiophene on the catalytically active surface of MoS 2: an ab initio local-density-functional study. Phys Rev Lett 80:1481
16. Song LJ, Pan MX, Qin YC, Xiu-Fang JU, Duan LH, Chen XL (2011) Selective adsorption desulfurization performance and adsorptive mechanisms of NiY zeolites. Chem J Chin Univ 32:787–792
17. Pieterse JAZ, Veefkind-Reyes S, Seshan K, Domokos L, Lercher JA (1999) On the accessibility of acid sites in ferrierite for pyridine. J Catal 187:518–520
18. Fan Y, Lu J, Shi G, Liu H, Bao X (2007) Effect of synergism between potassium and phosphorus on selective hydrodesulfurization performance of Co–Mo/Al_2O_3 FCC gasoline hydro-upgrading catalyst. Catal Today 125:220–228
19. Scholten JJF, Pijpers AP, Hustings AML (1985) Surface characterization of supported and nonsupported hydrogenation catalysts. Catal Rev 27:151–206
20. Yang X et al (2014) Impact of mesoporous structure of acid-treated clay on nickel dispersion and carbon deposition for CO methanation. Int J Hydrogen Energy 39:3231–3242
21. Li M et al (2011) Influence of modification method and transition metal type on the physicochemical properties of MCM-41 catalysts and their performances in the catalytic ozonation of toluene. Appl Catal B 107:245–252